RMetS
Royal Meteorological Society

A planetary-scale land–sea breeze circulation in East Asia and the western North Pacific

Wan-Ru Huang,[a]* Johnny C. L. Chan[a] and Shih-Yu Wang[b]

[a]*Guy Carpenter Asia-Pacific Climate Impact Centre, School of Energy and Environment, City University of Hong Kong, Hong Kong, China*

[b]*Utah Climate Center, Utah State University, Logan, Utah, USA*

*Correspondence to: W.-R. Huang, Guy Carpenter Asia-Pacific Climate Impact Centre, School of Energy and Environment, City University of Hong Kong, Tat Chee Ave., Kowloon, Hong Kong, China.
E-mail: wrhuang@cityu.edu.hk

The diurnal wind variation over the East Asian continent is commonly considered to be a combination of a land-sea breeze near the coast and a mountain–valley breeze along the slopes of the Tibetan Plateau. The local land–sea breeze along the coastline typically spans <100 km into the ocean. However, a detailed examination of the global reanalysis data suggests that this local land–sea breeze circulation apparently couples with the global-scale diurnal atmospheric pressure tide to produce a planetary-scale land–sea breeze with a spatial scale of ∼1000 km over the western North Pacific. Computations of the momentum budget and equivalent potential temperatures indicate that the atmospheric diurnal tidal wave contributes the most to this circulation feature. A diagnosis of the water vapour budget further suggests that the convergence of water vapour flux, which is related to the convergence of low-level wind induced by the seasonal change of diurnal tidal wave, leads to different times of occurrence of maximum diurnal rainfall over East Asia between summer and winter. Copyright © 2010 Royal Meteorological Society

Key Words: diurnal wind variation; diurnal rainfall variation; pressure tidal wave

Received 10 January 2010; Revised 15 April 2010; Accepted 1 June 2010; Published online in Wiley Online Library 16 August 2010

Citation: Huang W-R, Chan JCL, Wang S-Y. 2010. A planetary-scale land–sea breeze circulation in East Asia and the western North Pacific. *Q. J. R. Meteorol. Soc.* **136**: 1543–1553. DOI:10.1002/qj.663

1. Introduction

The periodic incoming solar heating in the atmosphere generates global tidal waves which can be revealed from variables such as pressure, wind, temperature, radiation fluxes, and even precipitation. The tidal waves evolve with periods of 24 and 12 h, commonly referred to as the diurnal and semi-diurnal oscillations respectively (Wallace and Hartranft, 1969; Haurwitz and Cowley, 1973; Hamilton, 1980; Hsu and Hoskins, 1989; Deser and Smith, 1998; Dai and Wang, 1999). On a regional scale, the pressure variations are geographically dependent and subject to the modulation of mountain–valley and land–sea differential heating, as well as latent heating in moist convection (Hamilton, 1981; Krishnamurti and Kishtawal, 2000; Ciesielski and Johnson, 2008). The East Asia–Western North Pacific (hereafter EAWNP) region with complex mountain–valley and land–sea distributions exhibits large diurnal variations in surface wind (Krishnamurti and Kishtawal, 2000; Yu *et al.*, 2008) and precipitation (Ramage, 1952; Zhao *et al.*, 2005; Dai *et al.*, 2007; Yu *et al.*, 2007a, 2007b; Li *et al.*, 2008; Zhou *et al.*, 2008). The diurnal surface wind variation is important for determining the timing of maximum diurnal precipitation (Yeh and Chen, 1998; Dai and Deser, 1999; Wu *et al.*, 2009). Compared to the extensive literature on the diurnal variation of precipitation, however, the diurnal variation of surface winds over the EAWNP region has attracted less attention.

During the summer months (June, July and August, or JJA), a typical diurnal variation of lower-tropospheric winds over the EAWNP region between morning (Figure 1(a)) and evening (Figure 1(b)), in terms of the 925 hPa

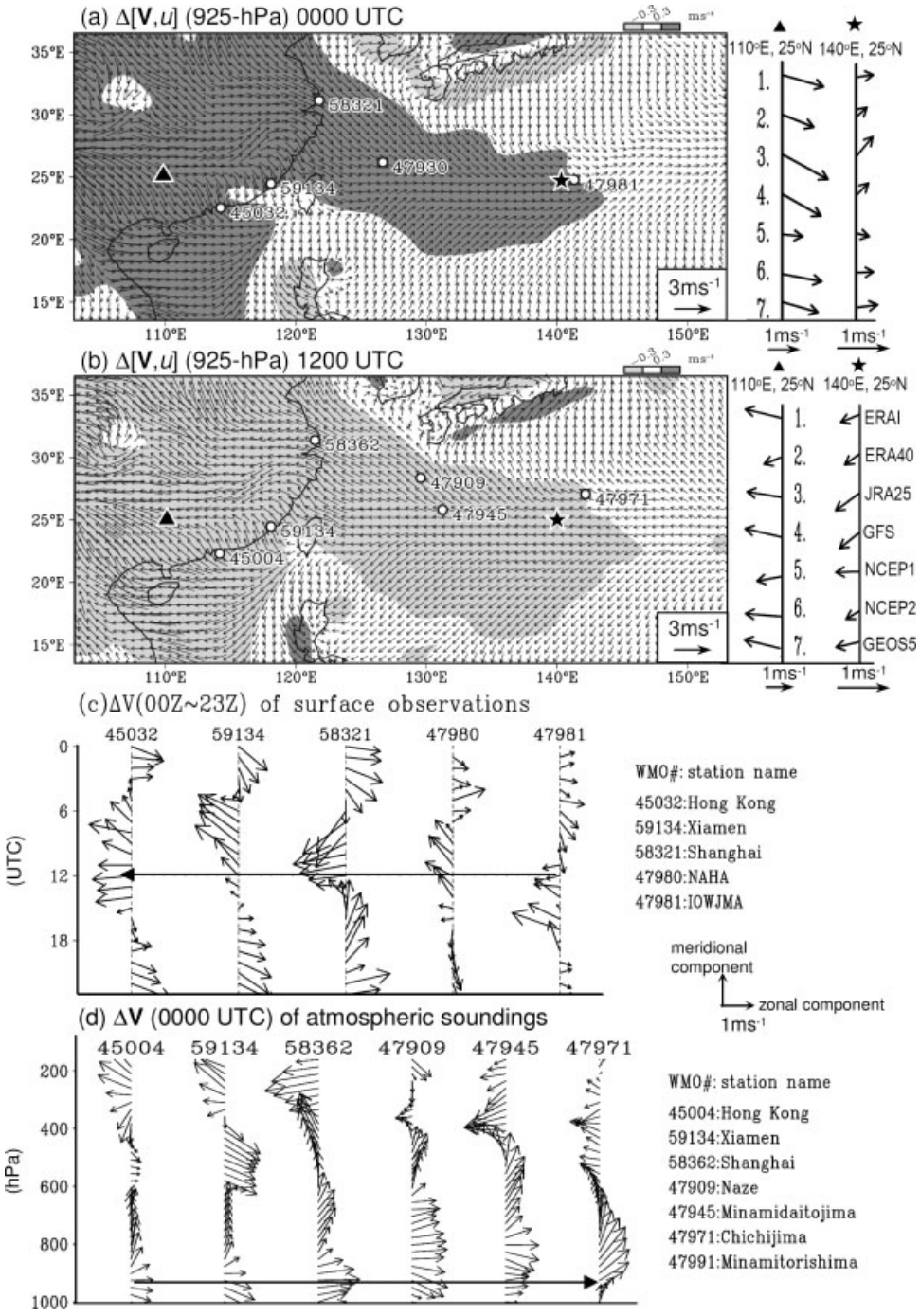

Figure 1. (a) The JJA mean of 925 hPa wind anomalies at 0000 UTC from GEOS5 (left panel) and two single-point wind anomalies ((110°E, 25°N) marked by triangle and (140°E, 25°N) marked by star) at 0000 UTC from seven reanalyses (right panel). (b) is similar to (a), but for 1200 UTC. The scale of stippled zonal wind speed is given atop (a)–(b). (c) The hourly surface wind anomalies of five selected surface stations in summer. (d) The multiple-level wind anomalies observed by six selected atmospheric soundings at 0000 UTC in summer. The WMO ID and name of selected stations (marked in (a)) and atmospheric soundings (marked in (b)) are provided in the right panel of (c) and (d). The scale of wind vector for (a)–(b) is given at bottom right and for (c)–(d) is shown in the right middle panel between them.

wind anomalies from the daily mean, reveals distinct features including the local land–sea breeze (hereafter LSB) circulation over the South China Sea and coastal East Asia, mountain–valley winds between the Tibetan Plateau and eastern China, and pronounced wind anomalies over the ocean between 120°E and 145°E. These features altogether form a planetary-scale LSB-like circulation which has not been examined in detail hitherto, although a concept of large-scale diurnal variation in the global surface winds was proposed in Dai and Deser (1999) based on the observations that surface wind divergence tends to peak in the morning over the major continents but in the late afternoon over the oceans. Previous studies suggested that a typical LSB circulation (e.g. LSB along the coast of the Philippines: Figure 1(a)–(b)), as a result of the difference in sensible heat flux over land and sea, only varies on a horizontal scale of <100 km (Schmidt, 1947; Neumann and Mahrer, 1971; Rotunno, 1983). In other words, to produce a diurnal variation of circulations of such a large scale as that revealed in Figure 1, an extra forcing mechanism in addition to the land–sea differential heating must exist. We therefore hypothesize that the pressure gradient force

from the large-scale global atmospheric pressure tidal wave is a major driving forcing of this planetary-scale LSB-like circulation.

The objective of the present study is to examine this hypothesis, which is important because a proper conceptual model for such a large-scale LSB-like circulation has significant implications for the improvement of weather and climate simulations. As the diurnal variation of low-level winds controls that of precipitation, this study also investigates how such a large-scale LSB-like circulation affects the diurnal precipitation change. Analyses are performed on both station data and global reanalyses, which are introduced in section 2. Results of this study are presented in sections 3 and 4, followed by a summary and discussion in section 5.

2. Data and Methodology

The analysis utilizes wind observations from surface stations (WMO ID and locations are given in Figure 1(a)), atmospheric soundings (located in Figure 1(b)), and meteorological data from seven global reanalyses including NCEP1, NCEP2, ERA40, ERAI, JRA25, GEOS5 and GFS (abbreviations and references described in Table I). The analysis covers the time period from 1989 to 2009 during summer (JJA) and winter (December, January and February, or DJF). The precipitation analysis uses the TRMM dataset (Tropical Rainfall Measuring Mission: Simpson *et al.*, 1996) which has been shown to resemble rain-gauge observations (Zhou *et al.*, 2008) with a good representation of the diurnal rainfall variability (Hong *et al.*, 2005). In addition, precipitation records of surface stations are extracted from the National Climatic Data Center†. Other information, including the period of record, temporal resolution and spatial resolution for all the datasets, is also listed in Table I.

In this study, anomalies of a given variable from the GEOS5 reanalyses, surface stations, and atmospheric soundings at a specific synoptic time step (e.g. 0000 UTC; 1200 UTC) are obtained by subtracting the daily means from their 3-hourly maps, 24-hourly observations, and twice-daily observations, respectively. The same procedure is carried out for the other reanalyses except that the map interval is 6 hours. The diurnal and semi-diurnal harmonic components of anomaly variables are obtained from Fourier analysis. Hereafter, the anomalies, diurnal (i.e. first harmonic) and semi-diurnal (i.e. second harmonic) cycles of a given variable X are denoted by ΔX, S1(X) and S2(X), respectively.

3. The Planetary-Scale LSB-like Circulation over the EAWNP Region

During the summer months, the planetary-scale LSB-like circulation in the morning (0000 UTC; 0700–0900 local standard time LST) (Figure 1(a)) exhibits westerly wind anomalies over the eastern Tibetan Plateau around 110°E and offshore winds up to 145°E. The reverse occurs in the evening (1200 UTC; 1900–2100 LST) (Figure 1(b)), with easterly wind anomalies spanning from 145°E westward to 100°E. Such a morning land-breeze-like and evening sea-breeze-like circulation covers a range of a few thousand kilometres between the coastline of East Asia (hereafter EA) and ∼145°E. This planetary-scale circulation is discernible not only in GEOS5 (left panel of Figure 1(a)–(b)) but in all other reanalyses (right panel of Figure 1(a)–(b)), surface stations (Figure 1(c)), and atmospheric soundings (Figure 1(d)). Because the results from all reanalyses are mutually consistent, to avoid redundancy we only show the GEOS5 reanalyses in the following discussion. The selection of GEOS5 is for two reasons. First, because the spatial resolution of GEOS5 (∼66.7 km in longitude ×50 km in latitude: Table I) is smaller than the horizontal scale of a typical LSB circulation (<100 km), GEOS5 is suitable for capturing features of local LSB which need to be resolved when we examine its possible coupling with the global atmospheric pressure tide later. Second, the 3-hourly GEOS5 data give a higher sampling rate for both the diurnal and semi-diurnal harmonics to be analysed than other 6-hourly reanalyses (Dai and Deser, 1999; Chen, 2005).

As revealed from the soundings over the EAWNP region (Figure 1(d)), the phase reversal of wind direction in the vertical implies ascending motion over the WNP ocean and downward motion over the EA continent which, subsequently, introduces a zonal mass flux circulation between the continent and the ocean. Because the differential heating between mountains and valleys only causes the diurnal wind change over land (Krishnamurti and Kishtawal, 2000) and the land–sea differential heating only induces LSB along the coast (Neumann and Mahrer, 1971), other forcing mechanisms for causing such a large-scale diurnal circulation must exist.

Dai and Deser (1999) proposed a mechanism responsible for a large-scale diurnal surface wind divergence change between day and night, which is similar to that for the large-scale monsoon circulation change between summer and winter. However, it takes weeks or even months to develop a giant thermal contrast between land and ocean that forms a monsoon system (e.g. Ramage, 1971). It is unlikely that the diurnally-driven land–sea thermal contrast can induce an LSB-like circulation on such a large scale within 12 hours. Deser and Smith (1998) examined the tropical oceanic zonal wind variations with the diurnal time-scale and suggested that the pressure gradient force (hereafter PGF) produced by the semi-diurnal component of atmospheric tides is likely the driving mechanism of such wind anomalies. It is therefore possible that the aforesaid extra forcing to induce a planetary-scale LSB-like circulation over the EAWNP region, as that shown in Figure 1, is linked to the diurnally varying global atmospheric pressure tide.

As seen from the distribution of mean sea-level pressure (hereafter SLP) anomalies, denoted as ΔSLP (Figure 2(a)), the global pressure tidal wave is a planetary-scale phenomenon dominated by a spatial wave-number-2 structure. It was noted that the pressure tidal wave experiences regular oscillations at the diurnal and semi-diurnal periods (Chapman and Lindzen, 1970). More than 96% of the total variability of global ΔSLP (Figure 2(a)) is explained by the combination of its diurnal S1(SLP) (Figure 2(b)) and semi-diurnal S2(SLP) (Figure 2(c)) harmonics. In general, ΔSLP over the tropical open ocean is mostly contributed by its related S2(SLP) and less by S1(SLP) (Dai and Wang, 1999). In the middle latitudes, the magnitude of ΔSLP is apparently larger over the EA

†Information is available at http://www.ncdc.noaa.gov/oa/climate/climatedata.html#hourly.)

Table I. List of observations and reanalysis datasets.

Dataset	Data period	Temporal resolution	Spatial resolution	Source information
WMO surface stations	1950 to present	Hourly		• http://dss.ucar.edu/datasets/ds564.0/
WMO sounding stations	1973 to present	Twice daily		• http://weather.uwyo.edu/upperair/sounding.html
Tropical Rainfall Measuring Mission (hereafter, TRMM)	1998 to present	3 hours	0.25° (long) ×0.25° (lat)	• Simpson *et al.* (1996)
National Centers for Environmental Prediction (NCEP)-NCAR Reanalysis (hereafter, NCEP1)	1948 to present	6 hours	2.5° (long) ×2.5° (lat)	•Kalnay *et al.* (1996) •http://dss.ucar.edu/datasets/ds090.0/
NCEP-Department of Energy Atmospheric Model Intercomparison Project (AMIP-II) Reanalysis (hereafter, NCEP2)	1979 to present	6 hours	2.5° (long) ×2.5° (lat)	•Kanamitsu *et al.* (2002) • http://dss.ucar.edu/datasets/ds091.0/
The European Centre for Medium- Range Weather Forecasts (ECMWF) Re-Analysis (hereafter, ERA40)	Sep 1957 to Aug 2002	6 hours	2.5° (long) ×2.5° (lat)	•Uppala *et al.* (2005) • http://dss.ucar.edu/datasets/ds120.0/
The ECMWF Interim Re-Analysis (hereafter, ERAI)	1989 to present	6 hours	0.702° (long) ×0.703° (lat)	•Simmons *et al.* (2007) • http://dss.ucar.edu/datasets/ds627.0/
Japanese 25-year Reanalysis Project (hereafter, JRA25)	1979 to present	6 hours	2.5° (long) ×2.5° (lat)	•Onogi *et al.* (2007) • http://dss.ucar.edu/datasets/ds625.1/
Goddard Earth Observing System Data Assimilation System Version 5 (hereafter, GEOS5)	1979 to Aug 2006	3 hours	0.667° (long) ×0.5° (lat)	• http://gmao.gsfc.nasa.gov/pubs/docs/GEOS5_104606-Vol27.pdf
NCEP Global Forecast System (hereafter, GFS)	June 2004 to present	6 hours	0.5° (long) ×0.5° (lat)	• Kanamitsu *et al.* (1991)

continent than the WNP region. Such distribution of ΔSLP can result in a positive longitudinal pressure gradient over the EAWNP region which has the same sign as the positive longitudinal pressure gradient associated with S1(SLP) (Figure 2(b)) but opposite sign to the negative longitudinal pressure gradient caused by S2(SLP) (Figure 2(c)). In other words, over the EAWNP region the land–sea difference of ΔSLP is more likely caused by S1(SLP) rather than S2(SLP). More information about the temporal–spatial evolutions of ΔSLP and its S1 and S2 harmonic modes were documented by Dai and Wang (1999) and Hoinka (2007).

The role of pressure tidal wave in affecting a large-scale LSB-like circulation over the EAWNP regions can be examined through the following momentum budget equation:

$$\frac{\partial V}{\partial t} = \underbrace{-f \bullet \mathbf{k} \times \mathbf{V}}_{\text{(CF)}} \underbrace{-\frac{1}{\rho}\nabla p}_{\text{(PGF)}} + \underbrace{\frac{\partial}{\partial z}(-V'w')}_{\text{(VDIF)}} + \underbrace{\text{residual}}_{\text{(RES)}}, \quad (1)$$

where $\boldsymbol{V}$, f, ρ, p and w are the atmospheric horizontal wind vector, Coriolis parameter, air density, pressure and the vertical velocity. $V'w'$ is the vertical turbulent flux of momentum, as defined in Holton (1992). Equation (1) consists of the Coriolis force term (hereafter, CF), the PGF term, the vertical diffusion term (VDIF), and the residual term (RES). Using these terms, wind variations can be reconstructed by integrating Eq. (1):

$$u = \int_{t-3}^{t} \left(fv - \frac{1}{\rho}\frac{\partial p}{\partial x} - \frac{\partial u'w'}{\partial z} + \text{residual}\right)\mathrm{d}t, \quad (2)$$

$$v = \int_{t-3}^{t} \left(-fu - \frac{1}{\rho}\frac{\partial p}{\partial y} - \frac{\partial v'w'}{\partial z} + \text{residual}\right)\mathrm{d}t. \quad (3)$$

In response to the temporal resolution of GEOS5, a 3 h time interval is used here for the time integration for the reconstructed winds. According to Eq. (2), the east–west land–sea distribution of S1(SLP) in Figure 2(b), which forms substantial longitudinal PGF between a high-pressure centre over the EA continent and a low-pressure centre over the WNP ocean (i.e. S1($-\partial p/\partial x$) >0), likely produces anomalous flows that resemble a giant land-breeze-like circulation (i.e. S1(u) >0). In contrast, the distribution of S2(SLP) in Figure 2(c) likely generates easterly wind anomalies over the EAWNP region, which is opposite to the offshore wind shown in Figure 1(a).

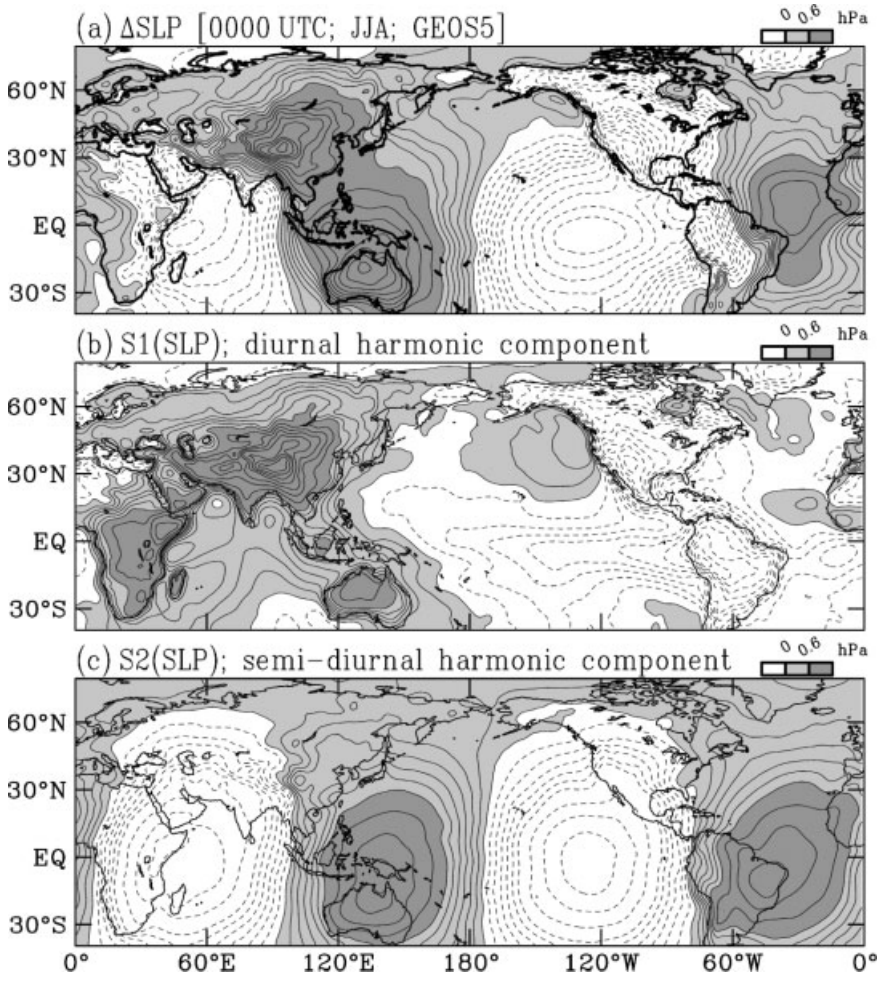

Figure 2. (a) The mean sea-level pressure anomalies (ΔSLP) for 0000 UTC of 1989–2009 summers (JJA) from GEOS5. (b) and (c) are the diurnal harmonic and semi-diurnal harmonic component of (a), respectively. The contour interval in all three panels is 0.1 hPa.

To examine which kinematic forcing term contributes most to the formation of large-scale LSB-like circulation, the 925 hPa wind anomalies induced by different forcing terms based on Eqs (2)–(3) are reconstructed. Because 23°–25°N is a latitudinal zone that reveals the furthest eastward extent of the east–west LSB-like circulation (Figure 3(a)), the reconstructed u-wind (denoted as u(forcing terms)) averaged over 23°–25°N is plotted in Figure 3(b) for a detailed discussion. Moreover, because u(RES) is two orders smaller than the other terms (not shown), we combine u(RES) together with u(VDIF) in Figure 3(b) for evaluation.

As revealed in Figure 3(a), the observed planetary-scale LSB-like circulation over the EAWNP region is mainly contributed by its diurnal component which explains more than 80% of the total variability of the zonal wind speed at 0000 UTC, based on the spatial variance of S1[u(925 hPa)] divided by that of Δ[u(925 hPa)] over the entire domain of Figure 3. Compared to the u(forces) at 23°–25°N (Figure 3(b)), u(PGF) has the same order as u(VDIF+RES) and is one order larger than u(CF) in both S1 and S2. This result suggests that CF is not important in forming the east–west LSB-like wind at 0000 UTC or 1200 UTC. However, Yu *et al.* (2008) found CF to be important for the meridional wind variations (not shown) that are related to the formation of the East Asia low-level jet over the EA continent. A further comparison between S1[u(PGF)] and S1[u(VDIF+RES)] shows that the former has an opposite direction but larger magnitude than the latter, indicating that S1(PGF) is the most important forcing source for S1[u(925 hPa)]. S2[u(PGF)], however, is almost cancelled out by S2[u(VDIF+RES)], resulting in a small variation of S2[u(925 hPa)] which contributes less than S1[u(925 hPa)] to the observed Δ[u(925 hPa)]. These results suggest that the kinematic forcing of the planetary-scale east–west LSB-like circulation over the EAWNP region is mainly caused by S1(SLP). While for areas where the meridional wind components are more evident than zonal wind components (e.g. the area (115°–120°E, 10°–20°N): Figure 3(a)), it is noted from the horizontal distribution of reconstructed (u, v) at 925 hPa (not shown) that CF and (VIDF+RES) are more important kinematic forcing terms as compared with PGF.

In addition to these dynamic forcing mechanisms, thermal forcing is also likely to have a contribution to the planetary-scale LSB-like circulation. Such a thermal forcing can be inferred from past studies regarding the formation of S1(SLP). It was noted that the global S1(SLP), which consists of migrating and non-migrating components, can be excited by orographic features and longitudinal variations in water vapour and ozone (Forbes and Garrett, 1979). Lindzen (1967) suggested that the major forcing of migrating tides is due to solar radiation absorption by water vapour in the troposphere and stratospheric ozone. Groves and Wilson (1982) further pointed out that water vapour heating provides a much larger contribution than ozone heating

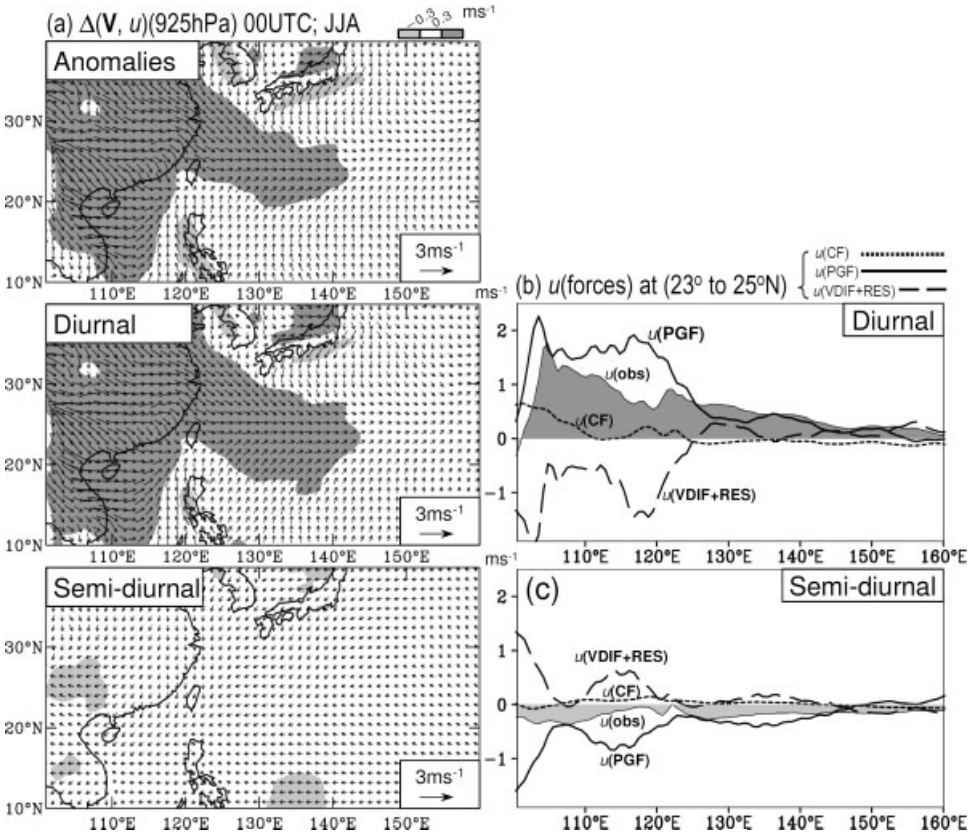

Figure 3. (a) The JJA mean of 925 hPa wind anomalies and its diurnal and semi-diurnal harmonic components at 0000 UTC from GEOS5. The scale of stippled zonal wind speed is given atop (a). Based on the momentum budget equation, zonal winds induced by the Coriolis force (i.e. u(CF)), pressure gradient force (i.e. u(PGF)) and vertical diffusion with residual terms (i.e. u(VDIF+RES)) are reconstructed and a 3 h time interval is used for the time integration. (b) The diurnal component of reconstructed and observed u-winds (i.e. u(obs)) averaged between 23°N and 25°N. (c) is similar to (b), but for the semi-diurnal component.

to migrating tides. In contrast to migrating tides, the non-migrating tides can be excited by latent heat released by meteorological events in the troposphere or longitudinal variations of sensible heat due to land–sea differences and topography (Hamilton, 1981; Kato *et al.*, 1982; Forbes and Groves, 1987; Tsuda and Kato, 1989). Lieberman and Leovy (1995) further indicated that sensible heat contributed the most to the non-migrating surface pressure tide. Because both the mountain–valley and land–sea differential heating are thermal forcing mechanisms that can excite the non-migrating component of S1(SLP), it is likely that the thermal forcing exciting the migrating component of S1(SLP) found by past studies (e.g. Lindzen, 1967; Groves and Wilson, 1982) is also generating the large-scale LSB-like circulation. Numerical experiments and analytical investigation will be needed to support this argument further.

4. Seasonal Variation of the LSB-like Circulation and Its Influence on Diurnal Rainfall

Because the thermally-driven global migrating tide follows the movement of the sun, seasonal variations in this migrating tidal wave should occur. Such a change implies a seasonal variation in S1(SLP) and subsequently a seasonal variation in the planetary-scale LSB-like circulation. It is noted that the basic structure of S1(SLP) (Figure 2(b)) is close to that of the diurnal harmonic of geopotential height (denoted as S1(Z)) at 925 hPa (Figure 4(a); JJA). To explore the seasonal variation of large-scale diurnal circulation, we examine both the differences of S1[Z(925 hPa)] (Figure 4(a)) and its related vertical cross-section of S1(Z) at 23°–25°N (Figure 4(b)) between summer and winter. A large dimension of high–low land–sea dipole structure appears in S1[Z(925 hPa)] over the EAWNP region during northern summer but this dipole disappears in winter (Figure 4(a)). The PGF related to the giant high–low land–sea dipole of S1[Z(925 hPa)] in summer can induce a planetary-scale land-breeze-like circulation over the EAWNP region, as suggested by Figure 3. However, due to the small dimension of high–low land–sea dipole of S1[Z(925-hPa)] over the EAWNP region in winter, only a very weak land-breeze-like circulation is observed (not shown).

Vertical cross-sections of S1(Z) averaged between 23° and 25°N during summer and winter are compared (Figure 4(b)) to explain further the seasonal difference of S1[Z(925 hPa)]. The basic structure of S1(Z) is a predominantly wave-number-1 pattern at the middle and upper troposphere, consistent with the major characteristics of global migrating tide as described in Chapman and Lindzen (1970). From summer to winter, this global migrating S1(Z), which can propagate downward to the surface over the WNP ocean, is shifted longitudinally ~60° westward (e.g. Chen *et al.*, 2001). Such a seasonal shift results in a sign change (from negative to positive) of S1(Z) over the WNP ocean from summer to winter. In the winter (summer) morning over the WNP ocean, the positive (negative) value of S1(Z) indicating a high (low) pressure system appears to limit (promote) the eastward extension of the land-breeze-like circulation from the coastline of EA to the WNP ocean. In contrast to the WNP ocean which is dominated by the

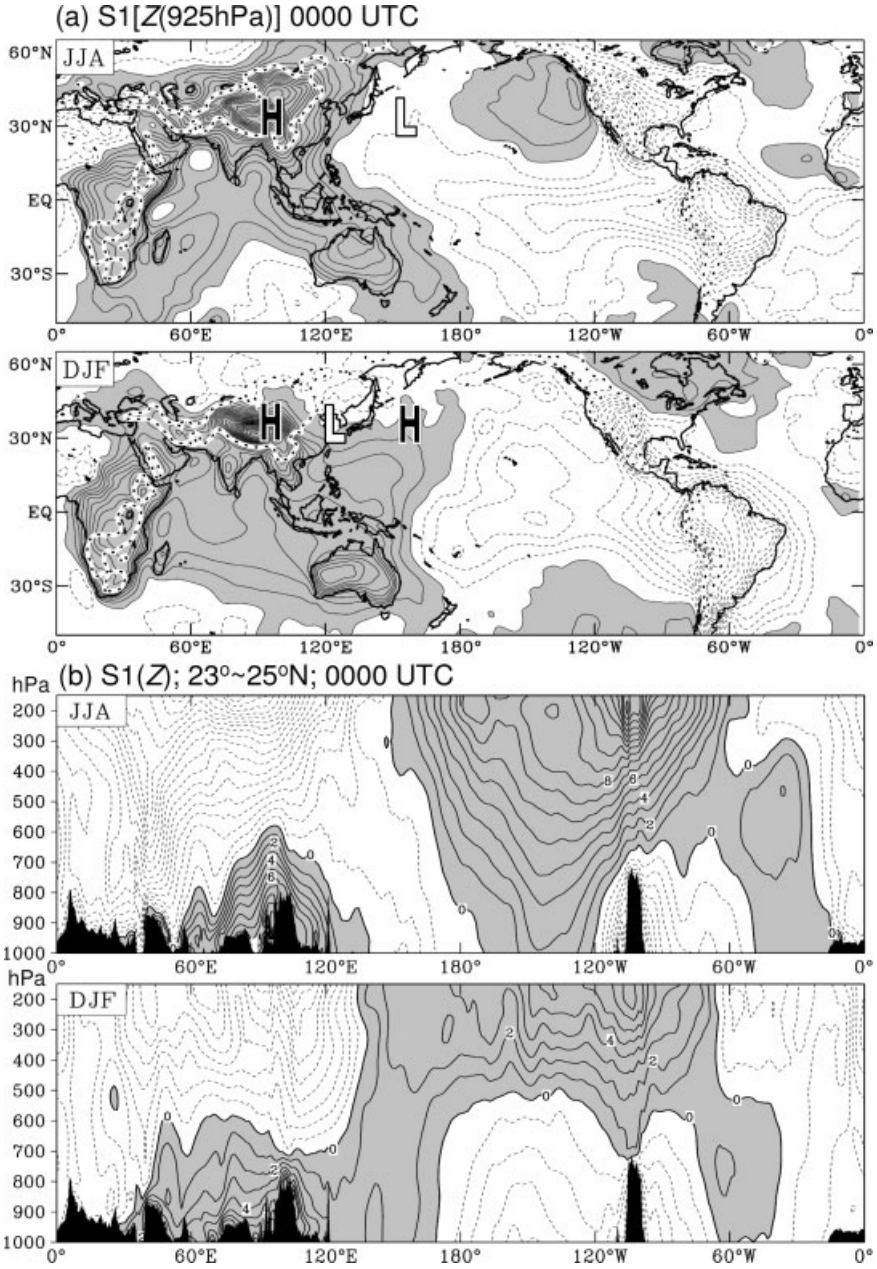

Figure 4. (a) The diurnal harmonic component of 925 hPa geopotential height S1[(*Z*(925 hPa)] at 0000 UTC for the 1989–2009 summer (JJA) and winter (DJF) periods. (b) The vertical cross-section of S1(*Z*) averaged between 23°N and 25°N. The contour intervals for S1(*Z*) in (a) and (b) are 1 metre. Positive areas of S1(*Z*) are stippled.

migrating tidal mode, the lower-tropospheric S1(*Z*) over the EA continent is controlled by the non-migrating tidal mode induced by the regional thermal forcings (Hsu and Hoskins, 1989; Chen *et al.*, 2001). The seasonally varying upper-troposphere downward propagating migrating tidal component combined with the lower-troposphere non-migrating tidal component forms a seasonally varying high–low land–sea dipole structure of S1[*Z*(925 hPa)] over the EAWNP region (Figure 4(a)) and, in turn, induces the change of the horizontal extent of the giant LSB-like circulation.

Next, we investigate the impact of the planetary-scale LSB-like circulation on the diurnal rainfall variation in EA by examining the variation of equivalent potential temperature (θ_e) because it consists of temperature and moisture changes that are important for exciting the global pressure tide (e.g. Forbes and Garrett, 1979). As seen from S1(θ_e) in Figure 5(a) (contoured), the lower tropospheric air over the ocean in the morning (0000 UTC) is noticeably warmer than that over the land. This land–sea difference of S1(θ_e) in the lower atmosphere agrees with the land–sea difference of S1[*Z*(925 hPa)] shown in Figure 4 because the warmer air lowers the atmospheric pressure. The warmer air depicted by positive values of S1(θ_e) covers a larger area of the WNP ocean in summer than in winter. Such a difference leads to the seasonal variation of S1(SLP) which causes a smaller LSB-like circulation in winter than in summer. Despite the seasonal difference, the unstable environmental situation indicated by positive values of S1($-\partial\theta_e/\partial z$) (shading in Figure 5(a)) over the ocean agrees with the fact that the precipitation over the sea tends to peak during the hours from late night to early morning (Kraus, 1963; Yang and Smith, 2006; Dai *et al.*, 2007). This feature of early morning maximum precipitation over the WNP ocean can be seen

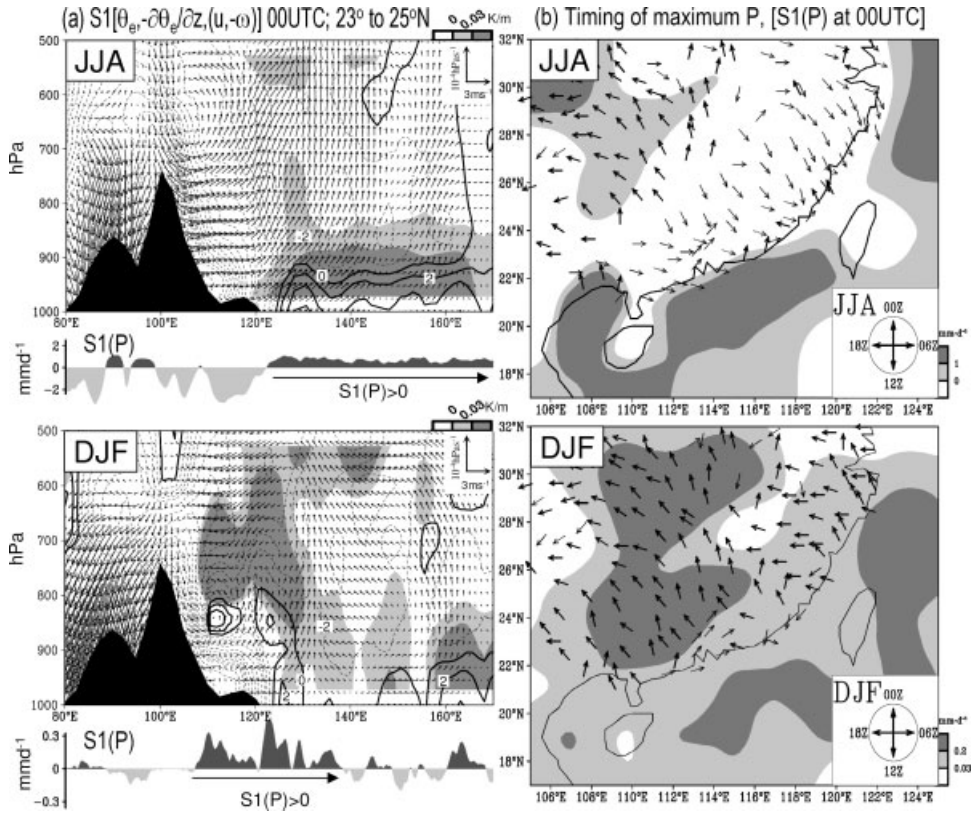

Figure 5. (a) The vertical cross-section of diurnal harmonic of equivalent potential temperature (θ_e; contoured), ($-(\partial\theta_e/\partial z)$; shaded), and ($(u, -\omega)$; vector) at 23°–25°N, 0000 UTC for the 1989–2009 summer and winter periods. The contour interval of θ_e is 5×10^{-2} K. The diurnal harmonic of precipitation (i.e. S1(P)) at 23°–25°N, 0000 UTC from TRMM 34B2 data production is shown in the bottom panel of (a). (b) The phase clock for the timing of maximum P within a day observed from surface stations is denoted by vectors and the positive areas of S1(P) at 0000 UTC are stippled with a scale given at right.

from the S1 component of precipitation, S1(P), at 0000 UTC as shown in Figure 5(a) (bottom panel) and Figure 5(b) (shading).

A seasonal difference of the diurnal cycle of precipitation in southern China, which was first noted in Li *et al.* (2008), can be revealed from both TRMM precipitation and surface observations (Figure 5(b)). This seasonal difference of S1(P) appears to be coherent with S1($-\partial\theta_e/\partial z$), the diurnal mode of moist static instability. As seen in Figure 5(a), the unstable areas with positive S1($-\partial\theta_e/\partial z$), which is distributed over the WNP ocean in summer, is shifted westward to the EA continent in winter and, in turn, causes the seasonal change of the LSB-like circulation. This westward shifting of S1($-\partial\theta_e/\partial z$) in the lower atmosphere causes the morning air over the EA continent to become more unstable and moist in the winter than in the summer. Consistent with the distribution of positive S1($-\partial\theta_e/\partial z$), S1($P$) over the EA continent reaches its maximum (minimum) in the winter (summer) morning. Such a seasonal timing difference of diurnal precipitation is not observed over inner China between 100° and 110°E where the effect of the shifting of the LSB-like anomalies circulation is small. These features of the diurnal precipitation timing as revealed in Figure 5(b) agree well with those observed previously (Zhao *et al.*, 2005; Yu *et al.*, 2007a, 2007b; Li *et al.*, 2008; Zhou *et al.*, 2008). Our finding on the difference of the planetary-scale LSB-like circulation between summer and winter therefore provides a dynamical explanation of the timing difference of diurnal precipitation between summer and winter in this region.

A more direct evidence for clarifying how an LSB-like circulation modulates the diurnal rainfall variation can be revealed by diagnosing the following water vapour budget equation:

$$P = E + (-\nabla \bullet Q) + (-\frac{\partial W}{\partial t}), \qquad (4)$$

where W, $\nabla \bullet Q$, P and E are the total precipitable water, the convergence or divergence of vertically integrated water vapour flux, the precipitation and the evaporation. Chen (2005) suggested that rainfall over EA is maintained by the water vapour supply through the convergence of water vapour flux (i.e. $P \sim (-\nabla \bullet Q)$). An examination of Eq. (4) at 1200 UTC over southeast Asia (SEA; boxed areas in Figure 6(a)), where there is larger diurnal rainfall variability, indicates that S1(P)$_{SEA}$ is mainly contributed by S1($-\nabla \bullet Q$)$_{SEA}$ (Figure 6(b)). On the other hand, it is found that the correlation coefficient between the temporal variations of S1(P)$_{SEA}$ and S1($-\nabla \bullet Q$)$_{SEA}$ is very high (∼0.94 in summer and ∼0.92 in winter), suggesting that the evolution of S1(P)$_{SEA}$ follows that of S1($-\nabla \bullet Q$)$_{SEA}$. Because the variation of S1($-\nabla \bullet Q$) is led by that of S1[($-\nabla \bullet V$)(925 hPa)] (e.g. Sui *et al.*, 1998), a sea-breeze-like circulation in Figure 1(b) likely results in the convergence of S1[($-\nabla \bullet V$)(925 hPa)], as well as the convergence of S1($-\nabla \bullet Q$), over the EA continent for supporting the positive values of S1(P) at 1200 UTC (Figure 6(c)).

Based on such a close relationship between S1(P), S1($-\nabla \bullet Q$) and S1[($-\nabla \bullet V$)(925 hPa)], further estimation for the contribution of seasonally varying S1(SLP) on affecting S1(P) over south China is made through estimating the contribution of seasonally varying S1(PGF) to the

change of S1[$(-\nabla \bullet V)$(925 hPa)]. Using Eqs (2)–(3), wind induced by different dynamic forcing terms are reconstructed for the calculation of S1[$(-\nabla \bullet V)$(925 hPa)]. As seen from Figure 7, S1[$(-\nabla \bullet V)$(925 hPa)] at 0000 UTC is primarily contributed by S1(PGF) and secondarily contributed by S1(CF) and S1(VDIF+RES) during both summer and winter. Corresponding to the seasonal change of the LSB-like circulation, S1[$(-\nabla \bullet V)$(925 hPa)] over south China changes from divergence in summer (Figure 7(b)) to convergence in winter (Figure 7(g)). This feature explains why in Figure 5 the S1(P) has an elevated structure over south China in winter but not in summer. Because S1[$(-\nabla \bullet V)$(925 hPa)] induced from S1(PGF) only affects S1(P), the highest percentage for the seasonal variation of S1(SLP) impacts on ΔP over south China should not exceed the percentage of S1(P) on explaining the variability of ΔP (~70%: Yin *et al.*, 2009).

Dai and Deser (1999) noted that the large-scale surface divergence/convergence is a major factor for modulating the diurnal rainfall over the oceans. Because a local LSB only appears over coastal regions or over big islands, there must be another reason different to the local LSB for causing the divergence/convergence over most of the WNP ocean where the local LSB does not exist. As seen from Figure 7, it is possible that the wind divergence/convergence induced by a large-scale LSB-like circulation leads to the diurnal modulation of rainfall over the WNP ocean.

In this study, a large-scale LSB-like circulation is suggested to be mainly induced by the PGF of S1(SLP) which involves a non-migrating component caused by local thermal forcing (Lieberman and Leovy, 1995). Because S1(P) is led by S1[$(-\nabla \bullet V)$(925 hPa)], the contribution of S1(P) from a local LSB that is induced by local thermal forcing might be estimated as:

$$\left[\frac{\text{Variance of S1(-}\nabla\bullet\text{ V) induced by the non - migrating component of S1(SLP)}}{\text{Variance of total S1}(-\nabla \bullet V)}\right]. \quad (5)$$

Haurwitz and Cowley (1973) indicated that the wave-number-1 component of S1(SLP) can be seen as migrating tidal wave, whereas the other wave numbers are called non-migrating tides. Based on Haurwitz and Cowley (1973), we extract the non-migrating component of S1(SLP) by removing its wave-number-1 component through a wave separation analysis. Then, similar to Figure 7, we calculate S1[$(-\nabla \bullet V)$(925 hPa)] induced by the non-migrating component of S1(SLP) for Eq. (5). An estimation of Eq. (5) area-averaged over SEA, an area marked in Figure 6(a), indicates that about 70% of S1[$(-\nabla \bullet V)$(925 hPa)] in summer is coming from its non-migrating component, consistent with Chen *et al.* (2001) that the non-migrating tidal wave is dominant over a major land mass. Such a result suggests that the LSB induced by local thermal forcing is important for modulating the diurnal rainfall over the EA continent. This suggestion does not contradict our earlier discussion regarding the role of LSB-like circulation in affecting S1(P) because the local LSB along the coast of EA is also part of the large-scale LSB-like circulation (see Figure 1). As for another selected area (125°–140°E, 21°–25°N) over the WNP ocean, about 40% of S1[$(-\nabla \bullet V)$(925 hPa)] is contributed by its non-migrating component, consistent with Chen *et al.* (2001) that the migrating tidal wave is dominant over oceans.

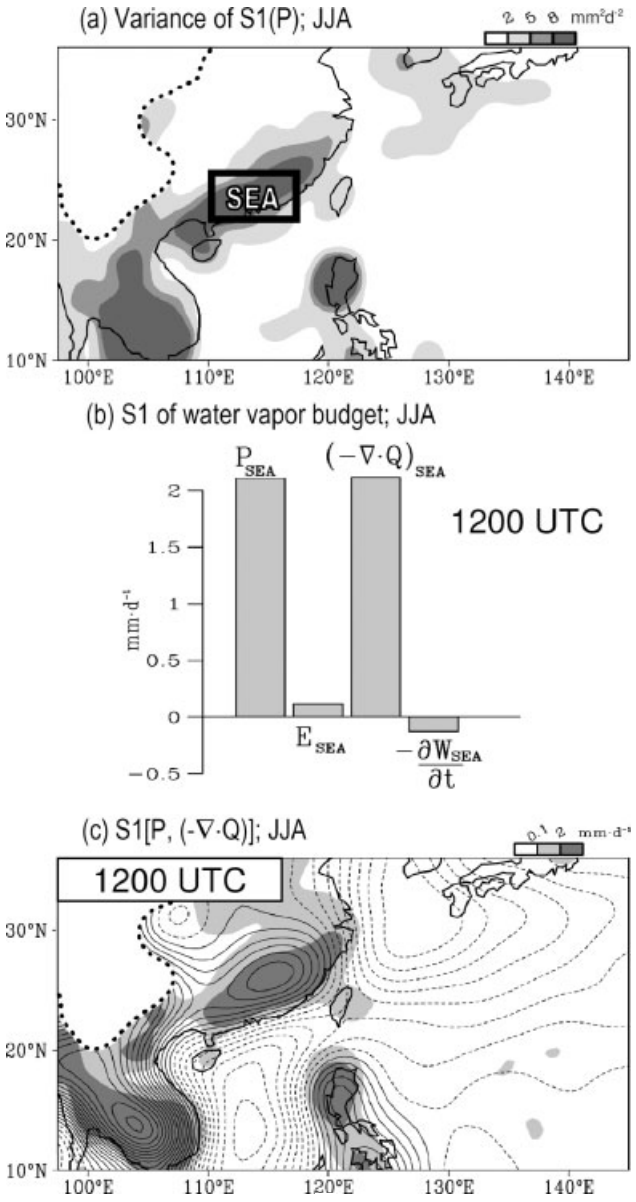

Figure 6. (a) Variance of 3-hourly S1(P) during the summer months. (b) Diagnosis of the water vapour budget extracted from GEOS5 for the maintenance of S1(P) at 1200 UTC area-averaged over southeast Asia (SEA, (110°–118°E, 21°–25°N), boxed areas in (a)) in summer. The evaporation, precipitable water, and convergence of water vapour flux are denoted by E, W, and $(-\nabla \bullet Q)$ in (b). (c) The JJA mean of S1(P) superimposed with S1 $(-\nabla \bullet Q)$ at 1200 UTC. The mountain areas in (b) are blocked. The contour interval of $(-\nabla \bullet Q)$ in (c) is 0.75 mm $\cdot d^{-1}$.

5. Conclusion

The diurnal wind variations over the EAWNP region consist of a mountain–valley breeze over the slopes of the Tibetan Plateau and an LSB near the coast, both of which are local features. A typical LSB is generally to be considered with a horizontal scale of less than 100 km (Neumann and Mahrer, 1971). Using the global reanalysis data, we find that these local diurnal circulations are apparently coupled with the global-scale diurnal tide and together produce a planetary-scale LSB-like circulation variation covering ~1000 km over the EAWNP region. The analysis of momentum budget indicates that the PGF produced from the diurnal harmonic of pressure tidal wave, i.e. S1(SLP), is the major dynamic forcing inducing this planetary-scale diurnal circulation

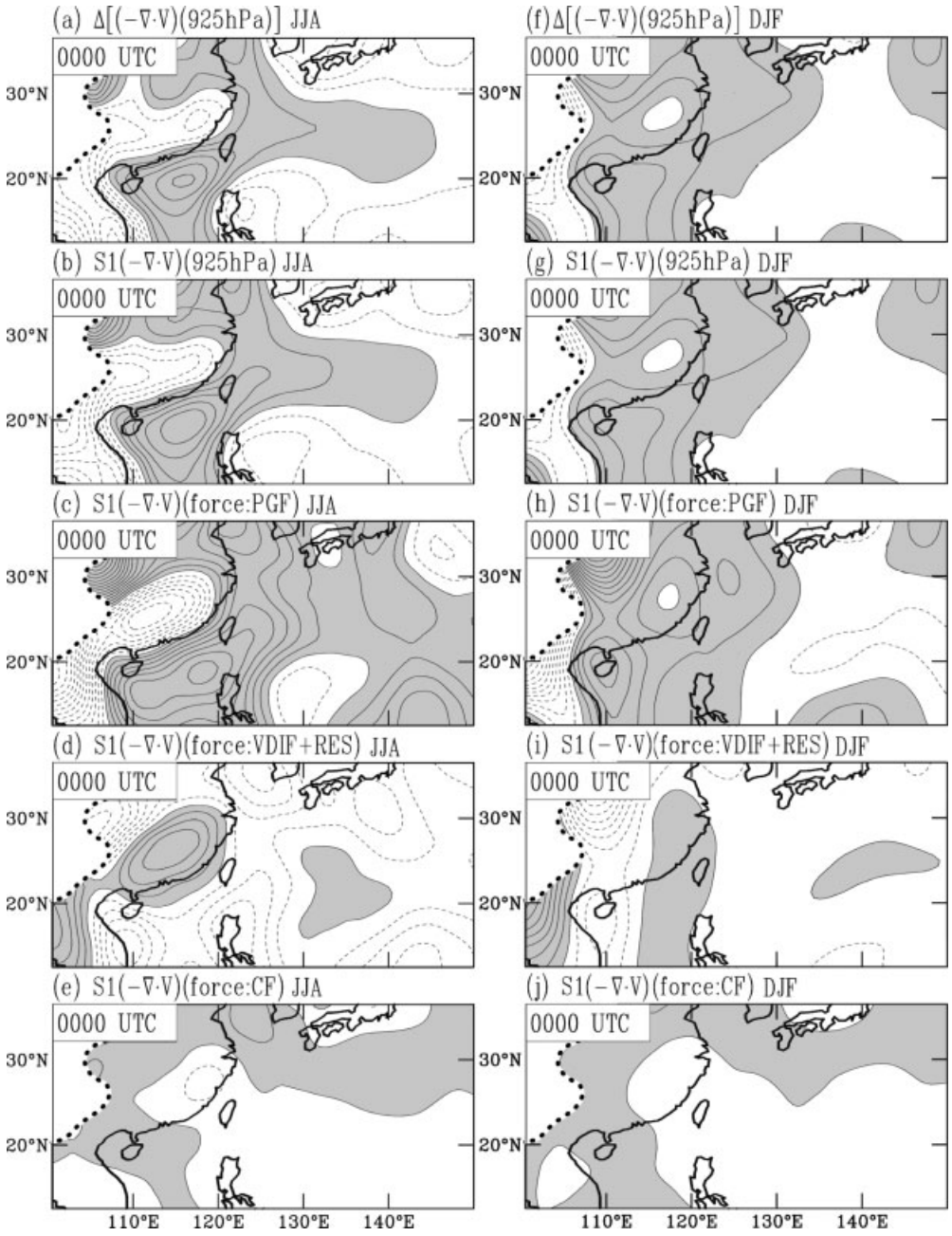

Figure 7. The JJA mean of (a) anomaly and (b) diurnal harmonic of 925 hPa wind convergence, i.e. $(-\nabla \bullet V)$, at 0000 UTC. The reconstructed S1$[(-\nabla \bullet V)$(925 hPa)] induced by (c) PGF, (d) VDIF+RES, and (e) CF. (f)–(j) are similar to (a)–(e), but for DJF. The contour interval in all panels is 5×10^{-7} s^{-1}.

feature. Moreover, we suggest that the thermal forcing exciting the migrating component of S1(SLP) (e.g. Lindzen, 1967; Groves and Wilson, 1982), in addition to the land–sea differential heating, helps generate this large-scale LSB-like circulation.

Pronounced seasonal variation of this planetary-scale LSB-like circulation between summer and winter is also found, with summer featuring broader coverage of the circulation. Such a seasonal difference is mainly caused by seasonal variations of the diurnal tidal wave, as inferred from the difference of S1(Z) between summer and winter. Examinations of equivalent potential temperature and water vapour budget further indicate that the seasonal varying θ_e causes the seasonal difference of LSB-like circulation which generates the surface convergence and leads to the seasonal change of water vapour convergence. This feature assists in the phase change of diurnal precipitation over the EA continent from the late afternoon peak in summer to the morning peak in winter, as noted in Li *et al.* (2008). Because the low-level circulation is important in representing the physical processes acting above the surface and controls the timing of the precipitation, this planetary-scale LSB-like circulation and the impact of such a circulation on the seasonal difference of diurnal precipitation timing deserve attention for future modelling research.

Acknowledgements

We thank two anonymous reviewers for their comments and suggestions which greatly improved the manuscript. SYW is supported by the USDA-CSREES funded Drought Management, Utah Project.

References

Chapman S, Lindzen RS. 1970. *Atmospheric tides.* D. Reidel: Dordrecht.

Chen T-C. 2005. Variation of the Asian monsoon water vapor budget: Interaction with the global-scale modes. Pp 417–459, chapter 10, in *The Asian monsoon*, Wang B (ed). Springer.

Chen T-C, Yen M-C, Schubert S. 2001. Diurnal variation of pressure-heights: A vertical phase shift. *J. Climate* **14**: 3793–3797.

Ciesielski PE, Johnson RH. 2008. Diurnal cycle of surface flows during 2004 NAME and comparison to model reanalysis. *J. Climate* **21**: 3890–3913.

Dai A, Deser C. 1999. Diurnal and semidiurnal variations in global surface wind and divergence fields. *J. Geophys. Res.* **104**: 31109–31125.

Dai A, Wang J. 1999. Diurnal and semidiurnal tides in global surface pressure fields. *J. Atmos. Sci.* **56**: 3874–3891.

Dai A, Lin X, Hsu K-L. 2007. The frequency, intensity, and diurnal cycle of precipitation in surface and satellite observations over low- and mid-latitudes. *Clim. Dyn.* **29**: 727–744.

Deser C, Smith CA. 1998. Diurnal and semidiurnal variations of the surface wind field over the tropical Pacific Ocean. *J. Climate* **11**: 1730–1748.

Forbes JM, Garrett HB. 1979. Theoretical studies of atmospheric tides. *Rev. Geophys. Space Phys.* **17**: 1951–1981.

Forbes JM, Groves GV. 1987. Diurnal propagating tides in the low-latitude middle atmosphere. *J. Atmos. Terr. Phys.* **49**: 153–164.

Groves GV, Wilson A. 1982. Diurnal, semi-diurnal and terdiurnal Hough components of surface pressure. *J. Atmos. Terr. Phys.* **44**: 599–611.

Hamilton K. 1980. The geographical distribution of the solar semidiurnal surface pressure oscillation. *J. Geophys. Res.* **85**(C4): 1945–1949.

Hamilton K. 1981. Latent heat release as a possible forcing mechanism for atmospheric tides. *Mon. Weather Rev.* **109**: 3–17.

Haurwitz B, Cowley AD. 1973. The diurnal and semidiurnal barometric oscillations, global distribution and annual variation. *Pure Appl. Geophys.* **102**: 193–222.

Hoinka KP. 2007. Semi-diurnal pressure fluctuation in the ERA40 data. *Meteorol. Z.* **16**: 255–260.

Holton JR. 1992. *An introduction to dynamic meteorology*. Academic Press: San Diego.

Hong Y, Hsu K-L, Sorooshian S, Gao X. 2005. Improved representation of diurnal variability of rainfall retrieved from the Tropical Rainfall Measurement Mission Microwave Imager adjusted Precipitation Estimation from Remotely Sensed Information using Artificial Neural Networks (PERSIANN) system. *J. Geophys. Res.* **110**: D06102, DOI:10.1029/2004JD005301.

Hsu H-H, Hoskins BJ. 1989. Tidal fluctuations as seen in ECMWF data. *Q. J. R. Meteorol. Soc.* **115**: 247–264.

Kalnay E, Kanamitsu M, Kistler R, Collins W, Deaven D, Gandin L, Iredell M, Saha S, White G, Woollen J, Zhu Y, Leetmaa A, Reynolds R, Chelliah M, Ebisuzaki W, Higgins W, Janowiak J, Mo KC, Ropelewski C, Wang J, Jenne R, Joseph D. 1996. The NCEP/NCAR 40-year reanalysis project. *Bull. Am. Meteorol. Soc.* **77**: 437–471.

Kanamitsu M, Alpert JC, Campana KA, Caplan PM, Deaven DG, Iredell M, Katz B, Pan H-L, Sela J, White GH. 1991. Recent changes implemented into the Global Forecast System at NMC. *Weather and Forecasting* **6**: 425–435.

Kanamitsu M, Ebisuzaki W, Woollen J, Yang S-K, Hnilo JJ, Fiorino M, Potter GL. 2002. NCEP–DOE AMIP-II Reanalysis (R-2). *Bull. Am. Meteorol. Soc.* **83**: 1631–1643.

Kato S, Tsuda T, Watanabe F. 1982. Thermal excitation of non-migrating tides. *J. Atmos. Terr. Phys.* **44**: 131–146.

Kraus EB. 1963. The diurnal precipitation change over the sea. *J. Atmos. Sci.* **20**: 551–556.

Krishnamurti TN, Kishtawal CM. 2000. A pronounced continental-scale diurnal mode of the Asian summer monsoon. *Mon. Weather Rev.* **128**: 462–473.

Li J, Yu R, Zhou T. 2008. Seasonal variation of the diurnal cycle of rainfall in southern contiguous China. *J. Climate* **21**: 6036–6043.

Lieberman RS, Leovy CB. 1995. A numerical model of nonmigrating diurnal tides between the surface and 65 km. *J. Atmos. Sci.* **52**: 389–409.

Lindzen RS. 1967. Thermally driven diurnal tide in the atmosphere. *Q. J. R. Meteorol. Soc.* **93**: 18–42.

Neumann J, Mahrer Y. 1971. A theoretical study of the land and sea breeze circulation. *J. Atmos. Sci.* **28**: 532–542.

Onogi K, Tsutsui J, Koide H, Sakamoto M, Kobayashi S, Hatsushika H, Matsumoto T, Yamazaki N, Kamahori H, Takahashi K, Kadokura S, Wada K, Kato K, Oyama R, Ose T, Mannoji N, Taira R. 2007. The JRA-25 reanalysis. *J. Meteorol. Soc. Jpn* **85**: 369–432.

Ramage CS. 1952. Diurnal variation of summer rainfall over east China, Korea and Japan. *J. Atmos. Sci.* **9**: 83–86.

Ramage CS. 1971. *Monsoon meteorology*. *International Geophysics Series*, Vol. 15. Academic Press: San Diego.

Rotunno R. 1983. On the linear theory of the land and sea breeze. *J. Atmos. Sci.* **40**: 1999–2009.

Schmidt FH. 1947. An elementary theory of the land- and sea-breeze circulation. *J. Atmos. Sci.* **4**: 9–20.

Simmons A, Uppala S, Dee D, Kobayashi S. 2007. '*ERA-Interim: New ECMWF reanalysis products from 1989 onwards.*' Pp 25–35 in Newsletter 110 – Winter 2006/07. ECMWF.

Simpson J, Kummerow C, Tao W-K, Adler RF. 1996. On the Tropical Rainfall Measuring Mission (TRMM). *Meteorol. Atmos. Phys.* **60**: 19–36.

Sui C-H, Li X, Lau K-M. 1998. Radiative–convective processes in simulated diurnal variations of tropical oceanic convection. *J. Atmos. Sci.* **55**: 2345–2357.

Tsuda T, Kato S. 1989. Diurnal non-migrating tides excited by a differential heating due to land–sea distribution. *J. Meteorol. Soc. Jpn* **67**: 43–54.

Uppala SM, Kållberg PW, Simmons AJ, Andrae U, da Costa Bechtold V, Fiorino M, Gibson JK, Haseler J, Hernandez A, Kelly GA, Li X, Onogi K, Saarinen S, Sokka N, Allan RP, Andersson E, Arpe K, Balmaseda MA, Beljaars ACM, van de Berg L, Bidlot J, Bormann N, Caires S, Chevallier F, Dethof A, Dragosavac M, Fisher M, Fuentes M, Hagemann S, Hólm E, Hoskins BJ, Isaksen L, Janssen PAEM, Jenne R, McNally AP, Mahfouf J-F, Morcrette J-J, Rayner NA, Saunders RW, Simon P, Sterl A, Trenberth KE, Untch A, Vasiljevic D, Viterbo P, Woollen J. 2005. The ERA-40 re-analysis. *Q. J. R. Meteorol. Soc.* **131**: 2961–3012.

Wallace JM, Hartranft FR. 1969. Diurnal wind variations, surface to 30 kilometers. *Mon. Weather Rev.* **97**: 446–455.

Wu P, Hara M, Hamada JI, Yamanaka MD, Kimura F. 2009. Why a large amount of rain falls over the sea in the vicinity of western Sumatra Island during nighttime. *J. Appl. Meteorol. Clim.* **48**: 1345–1361.

Yang S, Smith EA. 2006. Mechanisms for diurnal variability of global tropical rainfall observed from TRMM. *J. Climate* **19**: 5190–5226.

Yeh H-C, Chen Y-L. 1998. Characteristics of rainfall distributions over Taiwan during the Taiwan Area Mesoscale Experiment (TAMEX). *J. Appl. Meteorol.* **37**: 1457–1469.

Yin S, Chen D, Xie Y. 2009. Diurnal variations of precipitation during the warm season over China. *Int. J. Climatol.* **29**: 1154–1170.

Yu R, Zhou T, Xiong A, Zhu Y, Li J. 2007a. Diurnal variations of summer precipitation over contiguous China. *Geophys. Res. Lett.* **34**: L01704, DOI:10.1029/2006GL028129.

Yu R, Xu Y, Zhou T, Li J. 2007b. Relation between rainfall duration and diurnal variation in the warm season precipitation over central eastern China. *Geophys. Res. Lett.* **34**: L13703, DOI:10.1029/2007GL030315.

Yu R, Li J, Chen H. 2008. Diurnal variation of surface wind over central eastern China. *Clim. Dyn.* **33**: 1089–1097.

Zhao Z, Leung LR, Qian Y. 2005. '*Characteristics of diurnal variations of precipitation in China for the recent years.*' Pp 24–26 in CLIVAR Exchanges No. 3, International CLIVAR Project Office, Southampton, United Kingdom.

Zhou T, Yu R, Chen H, Dai A, Pan Y. 2008. Summer precipitation frequency, intensity, and diurnal cycle over China: A comparison of satellite data with rain gauge observations. *J. Climate* **21**: 3997–4010.

